Int. J. Multiphase Flow Vol. 14, No. 3, pp. 305–320, 1988
Printed in Great Britain

0301-9322/88 $3.00 + 0.00
Pergamon Press/Elsevier

A CAPACITANCE SENSOR FOR TWO-PHASE VOID FRACTION MEASUREMENT AND FLOW PATTERN IDENTIFICATION

J. J. M. GERAETS† and J. C. BORST‡
Laboratory for Aero- and Hydrodynamics, Delft University of Technology, Delft, The Netherlands

(*Received* 16 *March* 1987; *in revised form* 2 *December* 1987)

Abstract—A capacitance sensor has been developed for measuring time-averaged void fractions in two-phase pipe flow. The electrode configuration consists of a helical cross capacitor in which is placed a dielectric tube. To render edge effects negligible guard electrodes are used. For annular and dispersed flow configurations theoretical calibration curves are derived by solving the Laplace equation. The thickness of the wall of the dielectric tube appeared to be a very important design parameter. For annular and stratified flow experimental curves are presented. For many practical flow situations the time-averaged void fraction can be determined with an absolute accuracy of ± 0.03. Due to the relatively long axial extension local void fraction measurements are not possible and for mixed flow patterns, such as intermittent flow with frothy slugs, the accuracy is less. The time-varying output signal is useful for flow pattern identification. The sensor is easy to machine and only a standard capacitance meter is needed.

INTRODUCTION

For testing the similarity criteria of horizontal two-phase flow (Chesters 1977), the flow of air and a water–glycerine mixture in a 50 mm dia tube is compared with a two-phase flow of helium and water in a 5 mm dia tube, rotating around a parallel axis (Geraets 1986, 1988). The effective gravity in the 5 mm tube is 113 times natural gravity. On behalf of the scaling tests an instrument has been developed for measuring the time-averaged void fraction α. To allow accurate comparisons the same method is to be used in the 5 and 50 mm tubes. The method must be simple and the meter must withstand severe environmental conditions since high centrifugal forces (up to 1200 natural gravity) and high pressures (up to 4 MPa) are to be dealt with. Moreover, the flow may not be disturbed by the meter and the meter must be suitable for comparing the two flows. Identification of the exact flow pattern is subordinated to the comparison of the two flows. Plug and slug flow patterns are therefore defined in a somewhat different way than usual. Detailed measurement of the flow pattern is hindered by the axial width of the sensor.

From the three main techniques for measuring mean phase content—radioactive absorption and scattering, direct volume measurement by quick-closing valves and impedance measurements—only the latter is relatively easy to use in a rotating system. The determination of void fraction from electric impedance measurements has been widely applied for gas–water mixtures. Many of the basic techniques are reviewed by Hewitt (1978). The major difficulty with the impedance gauges is the sensitivity to flow pattern. This paper pays attention to this problem. If impedance gauges are operating in conditions in which conductance is dominant, drift occurs due to changes in liquid conductivity. For water an increase in temperature from 25 to 50°C doubles the conductivity, whereas the relative permittivity decreases by only 15%. Moreover, the relative permittivity of the water is not affected by a change of ionic concentration. Drift can be reduced by operating at sufficiently high frequency to give domination by capacitance. In this study a capacitance meter (Boonton 72BD) with a phase-sensitive detector, operating at a frequency of 1 MHz, is used. The accuracy of the measurement with the 5 and 50 mm sensors is better than 1.5%, as long as the specific conductivity of the liquid is $< 0.5\ 10^{-2}\ 1/\Omega\,\mathrm{m}$.

Capacitance sensors with different electrode configurations have been examined by Gregory & Scott (1973), Abouelwafa & Kendall (1980) and Borst (1983). The helical configuration seems to give the best results. Two thin brass strips are wound helically around a thin acrylate pipe section

†‡Present addresses: †Oce Nederland B. V., P.O. Box 101, 5900 MA Venlo and ‡Tidal Waters Division, P.O. Box 20904, 2500 EX The Hague, The Netherlands.

in such a way that they are always opposite each other. Abouelwafa & Kendall (1979) showed that the relation between the capacitance and the void fraction is linear and independent of the flow pattern and relative permittivity of the media. For the acrylate inner tube a correction factor is introduced which decreases with decreasing thickness of the tube. In contrast with the work of Abouelwafa & Kendall (1979) it is shown in this study that the thickness and relative permittivity of the acrylate tube are very important design quantities, especially for media with a high relative permittivity such as water.

DESIGN AND CONSTRUCTION OF THE SENSOR

The 5 and 50 mm sensors are geometrically similar. The similarity of the sensors has the advantage that the calibration curves are very alike and accurate comparisons of the flows are possible.

A photograph of the 50 mm sensor and the acrylate inner tube with electrode 2 is given in figure 1. Tape with a copper coating is wound around the tube which has an i.d. of 50 mm. Electrode 1 makes three complete revolutions around the tube, electrode 2 only two. The pitch of the helix is πD, hence the active length of the sensor is $2\pi D$ (≈ 6 dia). Between the electrodes, two shield electrodes are wound around the tube. The shield electrodes fix stray capacitance and make an analytical approach of the helical cross-capacitor possible. At both ends of electrode 2 a guard electrode is placed to render edge effects negligible (Heerens & Vermeulen 1975). The guard electrodes are connected electrically to the two shield electrodes. The acrylate tube is placed inside a stainless steel pipe (the shield tube) with the appropriate flanges. To prevent rupture of the sensor tube the space between the sensor tube and the shield tube is maintained at the operating pressure.

Miniature coaxial cable connectors are screwed into the thread ports of the shield tube in such a way that the spring-loaded centre wire of the coaxial connector makes contact with the electrode. The shield of the coaxial cable is connected to the shield tube, the shield electrodes and the guard electrodes. Using this arrangement the measured capacitance is independent of the length of the coaxial leads and external fields. The parasitic capacitance C_1 between electrode 1 and the shield and guard electrode is shunted by a low impedance voltage source V_0, see figure 2. By using the detector d as a zero-indicating instrument (V_1 can be adjusted), the parasitic capacitance C_2 between the shield/guard electrode and ground, does not affect the accuracy, only the bridge sensitivity. The same arguments can be used in the part of the bridge with the reference capacitor C_r.

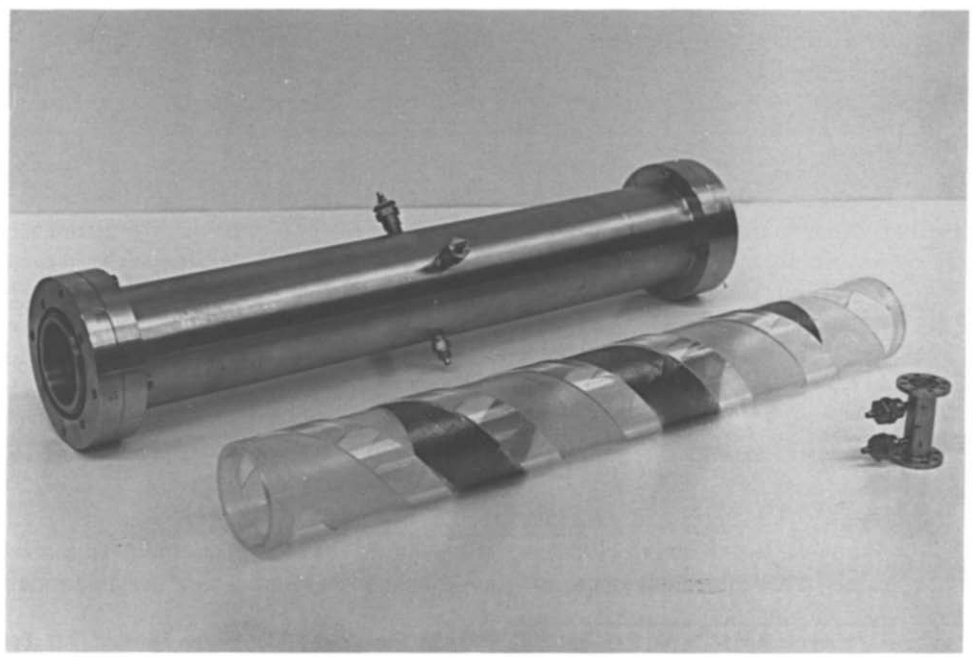

Figure 1. The 5 and 50 mm sensors.

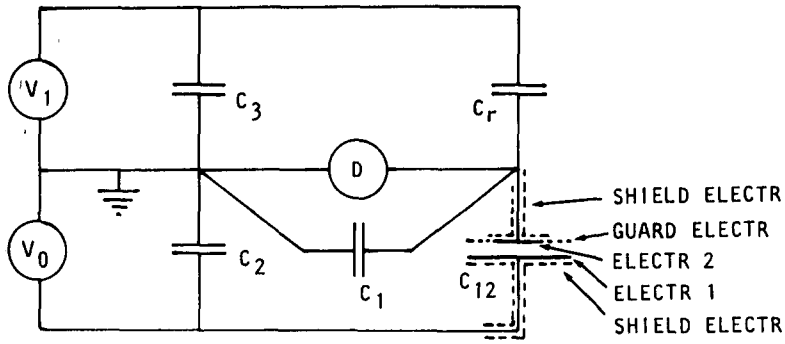

Figure 2. Bridge circuit for eliminating parastic capacitances.

The manufacturing of the 5 mm sensor is different from the procedure described above. Now the starting point is a stainless steel rod in which deep helical grooves are machined, see figure 3. The rod with grooves is cemented in a stainless steel tube with the appropriate flanges and thread ports for the electrical connections. The two shield electrodes and guard electrodes are connected to the shield tube by small stainless steel pins. Next the hole for the two-phase flow is drilled centrally into the rod in such a way that electrodes 1 and 2 are severed from the shield electrodes. The electrodes are then totally embedded in the insulating cement, see figure 3. Finally, the acrylate inner tube with the appropriate inner and outer diameter is cemented into the tube. The sensors machined in this way can withstand high pressures and high mechanical loads. A detailed description of the sensors is given by Borst (1985).

To survey the influence of the pitch and width of the helical electrodes on the sensor capacitance, a relatively simple electrode configuration with electrodes flush on the wall is examined analytically. The cross-section for $z = 0$ is depicted in figure 4, where z is the co-ordinate in the axial direction. To electrode 1 a potential of V_0 volt is applied, electrode 2 and the shield electrodes are connected to ground. At any cross-sectional plane the electrode configuration is identical except for an angular rotation z/pR. The pitch parameter p is equal to the ratio of the pitch s of the helix and the circumference $2\pi R$: $p = s/2\pi R$, where R is the inner diameter of the capacitor.

The potential distribution V at the electrodes is given by

$$\begin{aligned} V &= V_0 \quad \text{for} \quad \left|\phi - \frac{z}{pR}\right| < \phi_1 \\ V &= V \quad \text{for} \quad \phi_1 < \left|\phi - \frac{z}{pR}\right| < \pi, \end{aligned} \qquad [1]$$

where ϕ is a co-ordinate in the circumferential direction. The Fourier expansion of the above distribution is

$$V(R, \phi, z) = \frac{V_0\phi_1}{\pi} + \frac{2V_0}{\pi}\sum_{n=1}^{\infty}\frac{\sin(n\phi_1)\cos\left[n\left(\phi - \frac{z}{pR}\right)\right]}{n}. \qquad [2]$$

For calculating the capacitance and electric field distribution the Laplace equation in cylindrical co-ordinates has to be solved:

$$\frac{\partial^2 V}{\partial r^2} + \frac{1}{r}\frac{\partial V}{\partial r} + \frac{1}{r^2}\frac{\partial^2 V}{\partial \phi^2} + \frac{\partial^2 V}{\partial z^2} = 0, \qquad [3]$$

where r is a co-ordinate in the radial direction.

For reasons of symmetry the distributions of the potential in any cross-sectional plane is the same except for an angular rotation z/pR. Hence to solve the Laplace equation, the variables are separated in the following way:

$$V(r, \phi, z) = T(r) \times L(\phi, z). \qquad [4]$$

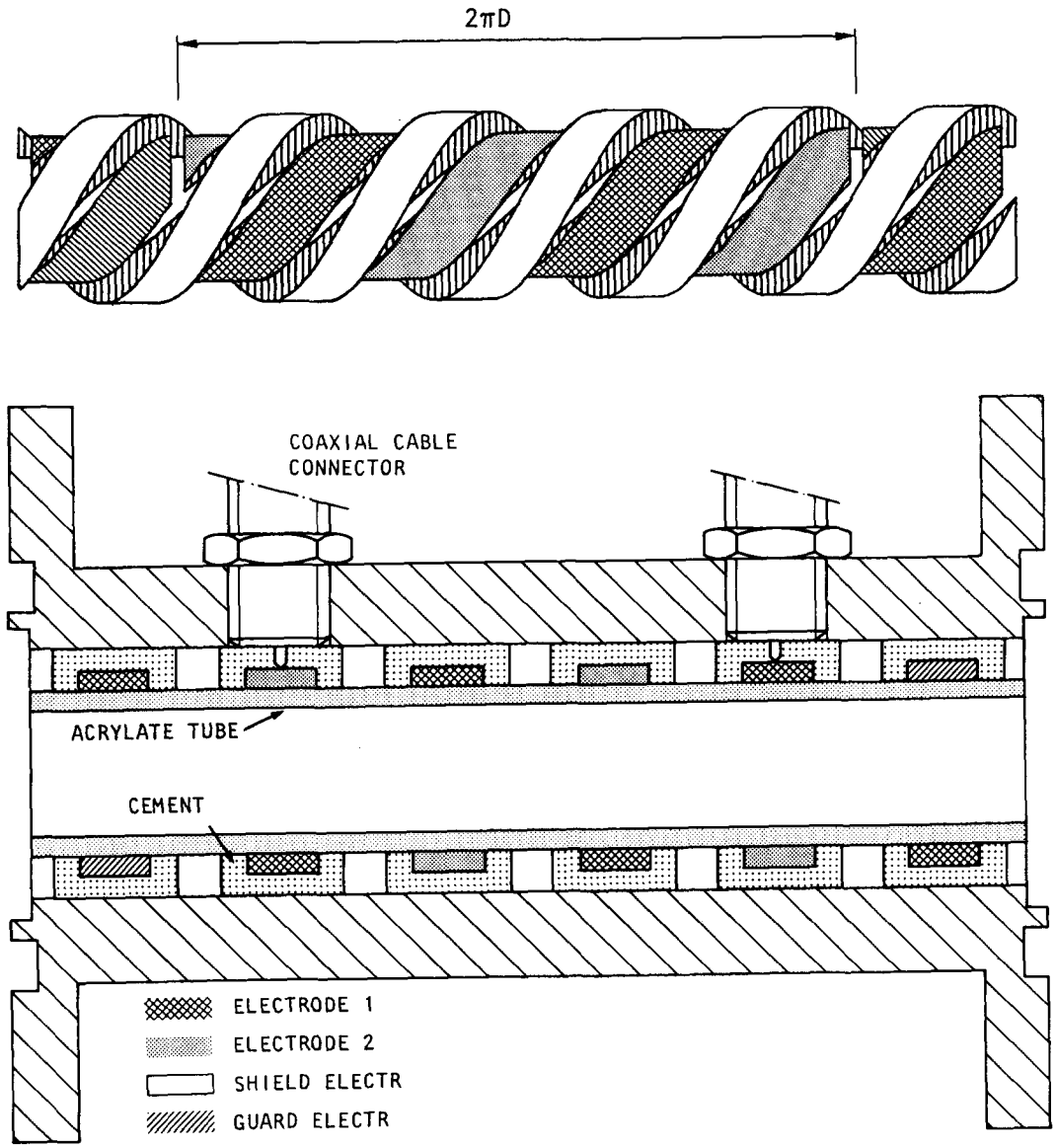

Figure 3. The 5 mm sensor and the helical electrode configuration.

Equation [3] then yields

$$\frac{1}{T}\left(\frac{d^2T}{dr^2}+\frac{1}{r}\frac{dT}{dr}\right)+\frac{1}{r^2L}\frac{\partial^2 L}{\partial\phi^2}+\frac{1}{L}\frac{\partial^2 L}{\partial z^2}=0. \qquad [5]$$

The general solution of the electrostatic potential distribution is

$$V=(A_0+B_0\phi+B_0'z)(C_0+D_0\ln z)$$
$$+\sum_{n=1}^{\infty}[A_n\cos(\sigma\phi-qz)+B_n\sin(\sigma\phi-qz)][C_nI_\sigma(qr)+D_nK_\sigma(qr)], \qquad [6]$$

where $I_\sigma(qr)$ and $K_\sigma(qr)$ are known as the modified Bessel functions of the first and second kind and of order σ. A_0, B_0, B_0', C_0, D_0, A_n, B_n, C_n and D_n are constants from integration. The necessity for V to be finite results in $D_n=0$ and the periodicity of the solution with respect to ϕ and z leads to $\sigma=m$, $q=n/pR$, $B_0=0$ and $B_0'=0$; m and n are integers. Symmetry of the solution with respect

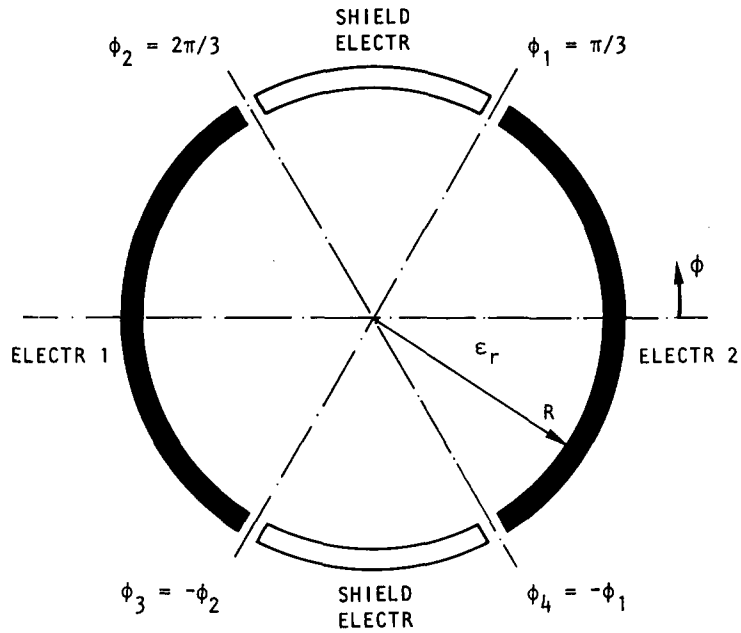

Figure 4. Cross-section of the helical cross-capacitor.

to $\zeta = 0$, where $\xi = \phi - z/pR$ results in $B_n = 0$. The potential now becomes

$$V(r, \xi) = F_0 + \sum_{n=1}^{\infty} F_n \cos(n\xi)\, I_n\left(\frac{nr}{pR}\right), \qquad [7]$$

where

$$F_0 = A_0 C_0 \quad \text{and} \quad F_n = A_n C_n.$$

Satisfying the boundary condition [2], the final solution is obtained (Borst 1985):

$$V(r, \xi) = \frac{\xi_1 V_0}{\pi} + \frac{2V_0}{\pi} \sum_{n=1}^{\infty} \frac{\sin(n\xi_1)\cos(n\xi) I_n\left(\frac{nr}{pR}\right)}{n I_n\left(\frac{n}{p}\right)}. \qquad [8]$$

The electric field E inside the helical cross-capacitor is calculated from

$$E_r = -\frac{\partial V}{\partial r}, \quad E_\phi = -\frac{1}{r}\frac{\partial V}{\partial \xi}\frac{\partial \xi}{\partial \phi}, \quad E_z = -\frac{\partial V}{\partial \xi}\frac{\partial \xi}{\partial z}. \qquad [9]$$

Figures 5 and 6 show the electric field in a cross-sectional plane and in an axial plane for a sensor filled with an homogeneous dielectric material. The length of the arrow is proportional to the magnitude of the component of the electric field in the cross-sectional plane. Large gradients of the electric field are present only in the neighbourhood of the shield electrodes. However, these field lines do not contribute to the capacitance. The internal cross-capacitance per unit length C' is

$$C' = \frac{1}{L}\left|\frac{Q}{V_0}\right| = \frac{1}{V_0}\int_{\phi_2}^{\phi_3} \epsilon_0 \epsilon_r E_{r=R} R \, d\phi, \qquad [10]$$

where Q is the electric charge on the electrode, L is the active length of the sensor, ϵ_0 is the permittivity of free space and ϵ_r is the relative permittivity of the medium between the electrodes.

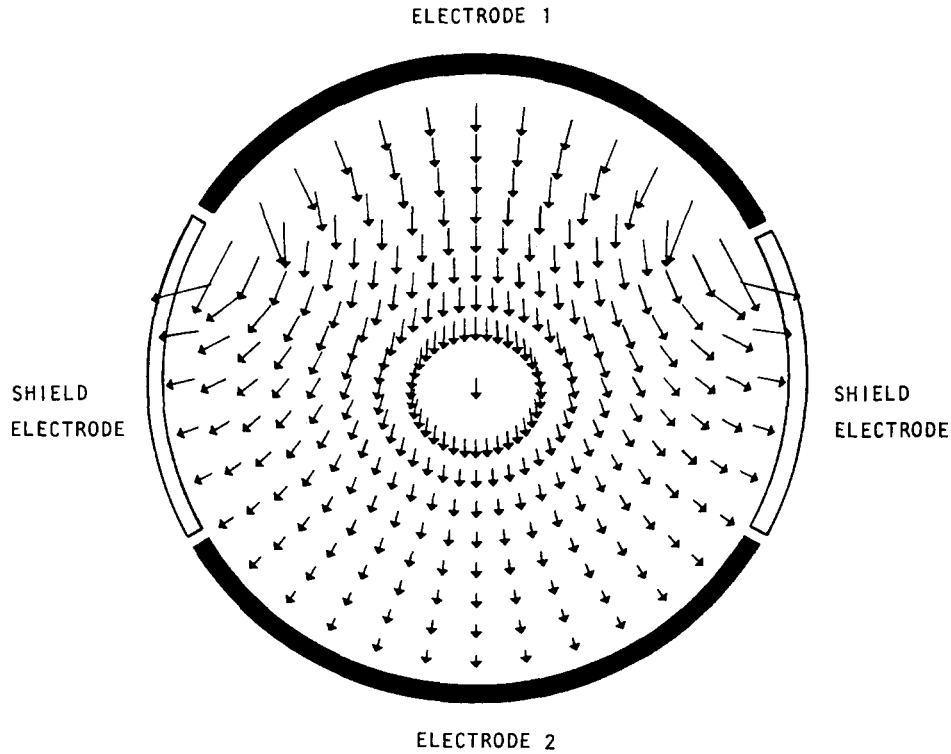

Figure 5. Electric field in a cross-sectional plane.

Using [8] and [9], the final expression for C' is

$$C' = \frac{2\epsilon_0\epsilon_r}{\pi}\left\{\ln\frac{\sin\left[\frac{(\phi_1+\phi_2)}{2}\right]}{\sin\left[\frac{(\phi_2-\phi_1)}{2}\right]} + \sum_{n=1}^{\infty}\frac{2\sin(n\phi_1)\sin(n\phi_2)I_{n+1}\left(\frac{n}{p}\right)}{pnI_n\left(\frac{n}{p}\right)}\right\}. \qquad [11]$$

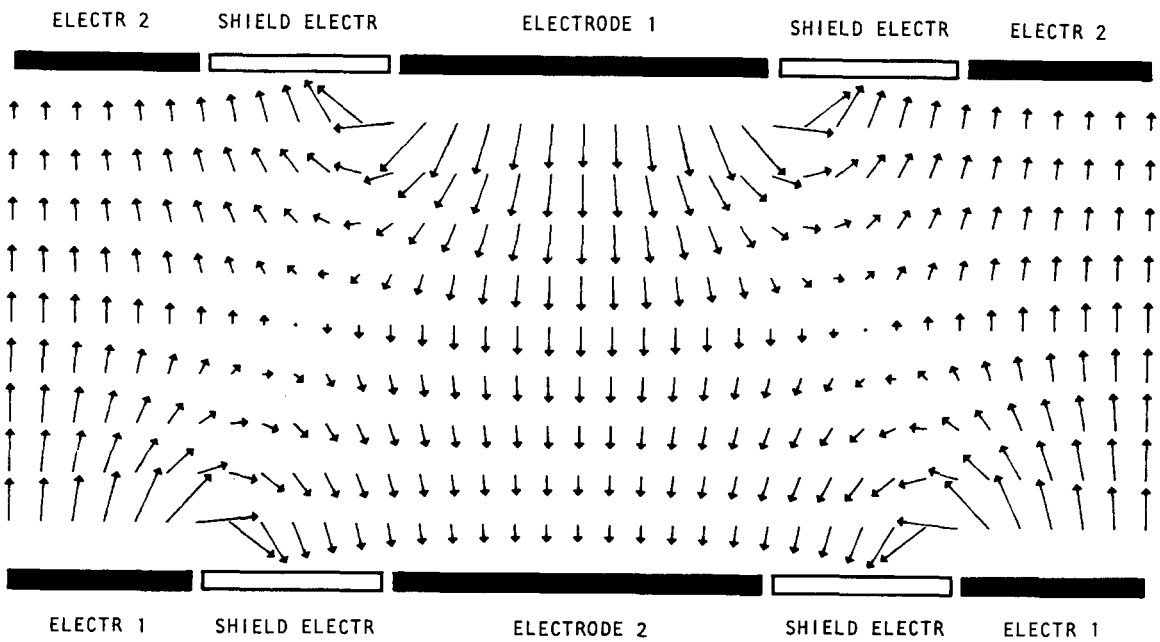

Figure 6. Electric field in an axial plane.

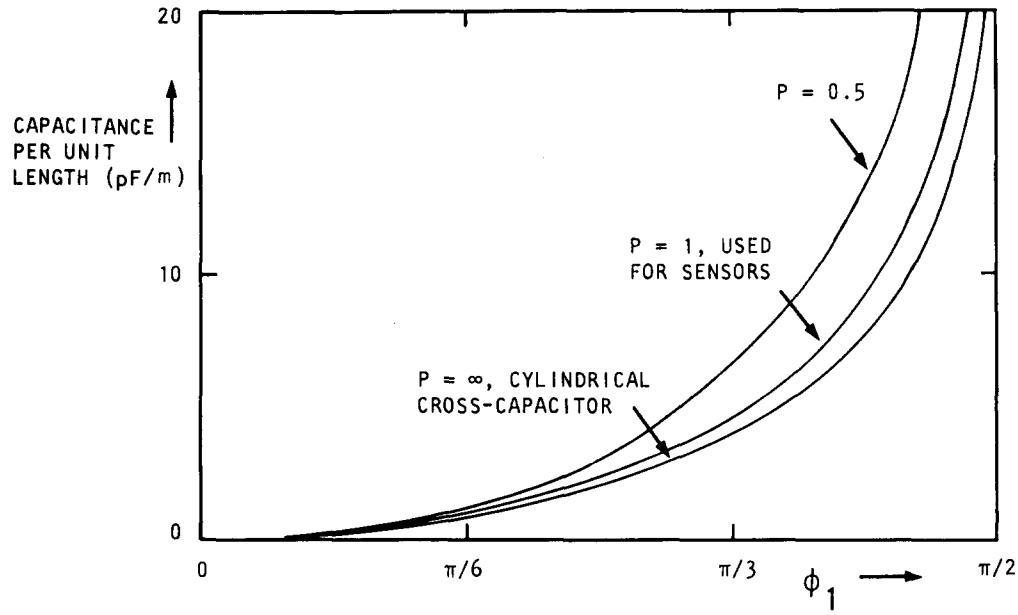

Figure 7. Capacitance per unit length of the helical cross-capacitor.

In figure 7 the capacitance per unit length as a function of the angle ϕ_1 ($2\phi_1 R$ is the width of the electrodes) for three values of the pitch parameter p is given. At large values of p the capacitance of the cylindrical cross-capacitor is obtained. At values of the pitch parameter >1 the influence of the helix form is small.

The 5 and 50 mm void sensors have the following design values: $\phi_1 = \pi/3$, $\phi_2 = 2\pi/3$, $p = 1$. The calculated capacitance per unit length is 4.54 pF/m. The measured capacitance of the 50 mm helix cross-capacitor deviates only 3% from the predicted value.

If the sensor is filled with an inhomogeneous dielectric material or a mixture of two dielectric materials the field lines will be distorted and, in general, the capacitance cannot be determined analytically. However in special cases, such as idealized annular flow or idealized dispersed bubble flow, an analytical approach is possible. In the following sections the capacitance of a cylindrical cross-capacitor (=helical cross-capacitor with $p = \infty$) is calculated for these two cases.

THEORETICAL AND EXPERIMENTAL CALIBRATION CURVES

For cylindrically symmetrical flow such as annular and dispersed flow the sensor may be modelled by a cylindrical cross-capacitor filled with symmetrically placed dielectric cylinders. The results and analysis for a helical cross-capacitor are almost the same but the algebraic efforts required are much greater. The capacitance of an idealized annular flow is calculated and compared with the experimental curves and the influence of the acrylate sensor tube is examined. Theoretical calibration curves for dispersed bubble flow and experimental curves for stratified flow are presented. Finally, the measurement strategy for intermittent flow is outlined.

Annular flow

Consider a cylindrical cross-capacitor of circular cross-section, as shown in figure 8. The configuration simulates an idealized annular flow (cylindrical symmetry and the absence of waves on the surface). The space inside the cylindrical electrodes is divided into three regions:

the gas core in region 1	$r < R_1$	and	$\epsilon = \epsilon_0\epsilon_1$
the liquid annulus in region 2	$R_1 < r < R_2$	and	$\epsilon = \epsilon_0\epsilon_2$
the sensor tube in region 3	$R_2 < r < R_3$	and	$\epsilon = \epsilon_0\epsilon_3$.

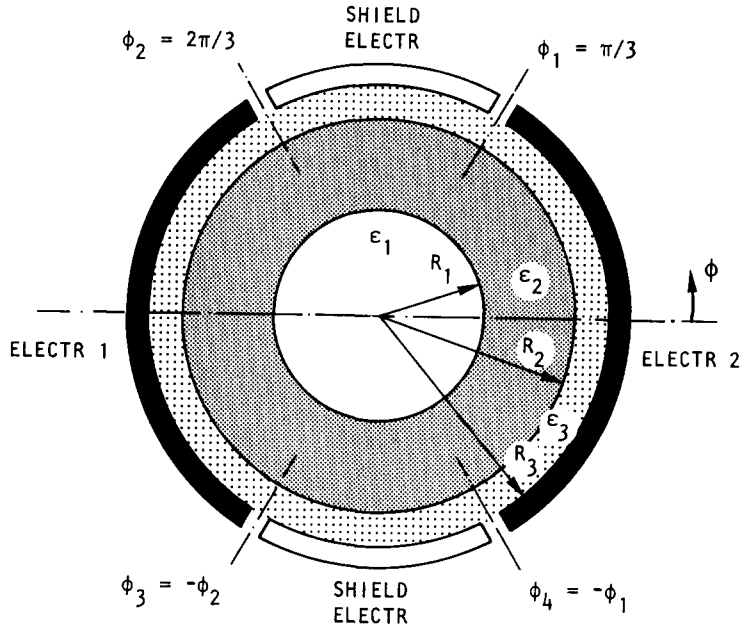

Figure 8. Cross-section of the cylindrical cross-capacitor.

Our objective is to calculate the internal cross-capacitance per unit length, C', between electrodes 1 and 2. To electrode 1 a potential of V_0 volt is applied, while electrode 2 and the shield electrodes are earthed. The Laplace equation in two dimensions in cylindrical co-ordinates is

$$\frac{\partial^2 V}{\partial r^2} + \frac{1}{r}\frac{\partial V}{\partial r} + \frac{1}{r^2}\frac{\partial^2 V}{\partial \phi^2} = 0. \qquad [12]$$

The general form of the electrostatic potential distribution within the capacitor is

$$V(r, \phi) = (A_0 + B_0\phi)(C_0 \ln r + D_0) + \sum_{n=1}^{\infty} \{(C_n r^n + D_n r^{-n})[A_n \cos(n\phi) + B_n \sin(n\phi)]\}. \qquad [13]$$

Taking into account the symmetry with respect to ϕ and the necessity for V to be finite, the expressions for $V(r, \phi)$ in the three regions are:

region 1 $$V_1(r, \phi) = A_{10} + \sum_{n=1}^{\infty} A_{1n} r^n \cos(n\phi) \qquad [14]$$

region 2 $$V_2(r, \phi) = A_{20} + B_{20} \ln r + \sum_{n=1}^{\infty} (A_{2n} r^n + B_{2n} r^{-n}) \cos(n\phi) \qquad [15]$$

region 3 $$V_3(r, \phi) = A_{30} + B_{30} \ln r + \sum_{n=1}^{\infty} (A_{3n} r^n + B_{3n} r^{-n}) \cos(n\phi). \qquad [16]$$

The boundary conditions for the problem are:
—equal potential at the boundary between

regions 1 and 2 $$V_1(R_1, \phi) = V_2(R_1, \phi) \qquad [17]$$

and

regions 2 and 3 $$V_2(R_2, \phi) = V_3(R_2, \phi); \qquad [18]$$

—potential distribution at the electrode surface obtained from [2] with $p = \infty$,

$$V_3(R_3, \phi) = \frac{V_0 \phi_1}{\pi} + \frac{2V_0}{\pi} \sum_{n=1}^{\infty} \frac{\sin(n\phi_1)\cos(n\phi)}{n}; \qquad [19]$$

—continuity of the radial component of the displacement at the boundary between

$$\text{regions 1 and 2} \qquad \epsilon_0\epsilon_1\left(\frac{\partial V_1}{\partial r}\right)_{r=R_1} = \epsilon_0\epsilon_2\left(\frac{\partial V_2}{\partial r}\right)_{r=R_1} \qquad [20]$$

and

$$\text{regions 2 and 3} \qquad \epsilon_0\epsilon_2\left(\frac{\partial V_2}{\partial r}\right)_{r=R_2} = \epsilon_0\epsilon_3\left(\frac{\partial V_3}{\partial r}\right)_{r=R_2} \qquad [21]$$

The solution of [16] with the help of [9] and [10] leads to the following expression for the capacitance per unit length:

$$C' = \frac{2\epsilon_0\epsilon_3}{\pi}\left\{\ln\frac{\sin\left[\frac{(\phi_1+\phi_2)}{2}\right]}{\sin\left[\frac{(\phi_2-\phi_1)}{2}\right]} - \sum_{n=1}^{\infty}\frac{4(\mathrm{ACF}_1^n + \mathrm{BD})\sin(n\phi_1)\sin(n\phi_2)}{n(\mathrm{CDF}_2^n + \mathrm{ABF}_3^n + \mathrm{ACF}_1^n + \mathrm{BD})}\right\}, \qquad [22]$$

where $A = \epsilon_1 + \epsilon_2$, $B = \epsilon_2 + \epsilon_3$, $C = \epsilon_3 - \epsilon_2$, $D = \epsilon_2 - \epsilon_1$ and $F_1 = (R_2/R_1)^2$, $F_2 = (R_3/R_2)^2$, $F_3 = (R_3/R_1)^2$.

For the special case $R_2/R_1 \approx 1$, $\epsilon_1 = \epsilon_3$ and $\epsilon_2 < 5$, a solution for the capacitance is also given by Rehman *et al.* (1982).

For prescribed values of ϕ_1, ϕ_2, ϵ_1, ϵ_2 and ϵ_3, [22] is only a function of R_2/R_3 and the void fraction $\alpha = (R_1/R_2)^2$: $C = f(\alpha, R_2/R_3)$. Since we are only interested in the relation between the relative capacitance difference, $\Delta C/\Delta C_0$, and the void fraction, the following expression has been calculated numerically:

$$\mathrm{RCD} = \frac{\Delta C}{\Delta C_0} = \frac{C_m - C_1}{C_2 - C_1} = f\left(\alpha, \frac{R_2}{R_3}\right), \qquad [23]$$

where RCD is the relative capacitance difference and C_1, C_2 and C_m are the capacitances of the cylindrical cross-capacitor filled with medium 1 (empty capacitor, $\alpha = 1$), medium 2 (liquid filled capacitor, $\alpha = 0$) or a mixture of media 1 and 2.

In figure 9 the results of the calculations for a water annulus ($\epsilon_2 = 80$) and an air core ($\epsilon_1 = 1$) are shown. The curves are very sensitive to the thickness of the acrylate sensor tube ($\epsilon_3 = 3.1$).

For $R_2/R_3 = 0.9$ the calculated curve is almost linear (with a glass sensor tube ($\epsilon_r = 7$) the most linear curve is obtained for $R_2/R_3 = 0.8$). The relative capacitance difference for the sensor with electrodes flush with the wall ($R_2/R_3 = 1$) is independent of the void fraction in the relevant void range $\alpha > 0.8$ and therefore not very useful. The electric field lines prefer going through the thin water annulus to the shield electrode rather than crossing the annulus via the gas core to electrode 2. This effect is suppressed by placing an inner cylinder with a low relative permittivity concentrically in the sensor. The calculated curves for an acrylate core differ by <0.02 (absolute units) from those for an air core.

The experimental calibration curves for annular flow qualitatively show the same influence of the thickness of the wall of the sensor tube, see figure 9. The gas core is simulated by symmetrically placed acrylate rods and the void fraction is calculated from the diameter of the rods. In the void range $0.2 < \alpha < 0.8$ the experimental points are 0.1–0.2 higher than the calculated ones.

The RCD with the rods placed against the wall of the sensor tube is about 0.05 smaller. Crossing of the field lines from electrode 1 to electrode 2 is hindered then. This indicates the non-linearity of the device.

The two sensors are mainly used for stratified and intermittent flow. Therefore the thickness of the acrylate tube is chosen in such a way that the curve for these flow types is as linear as possible ($R_2/R_3 = 0.88$ for the 50 mm section and $R_2/R_3 = 0.92$ for the 5 mm section). In the relevant void range for annular flow, $\alpha > 0.8$, the calibration points are reasonably close to the diagonal.

The diagonal in figure 9 represents filling of the sensor in the vertical position. The measurements for vertical filling of the sensor deviate by <0.02 from the diagonal, including the edge regions. This result indicates that the sensor is uniform in the axial direction and that the guard electrodes effectively suppress edge effects.

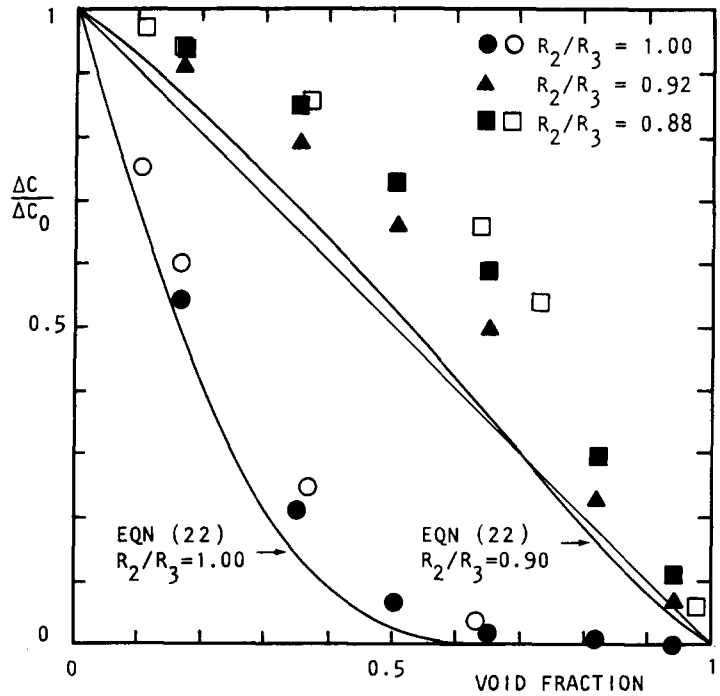

Figure 9. Calibration curves for annular flow: 50 mm (open symbols); 5 mm (closed symbols).

If a liquid with a low relative permittivity value ($\epsilon_r < 5$) is used, the theoretical and experimental calibration curves are more linear and almost independent of the thickness of the dielectric sensor tube (Borst 1985).

Dispersed flow

In the past many solutions for the relative permittivity (and conductivity) of a bulk phase containing spheres with a different permittivity have been presented. The various solutions are all derived by solving the Laplace equation. Maxwell (1881) considered spheres of uniform size, located in the bulk phase and found that if the permittivity of the spheres is small compared to the permittivity of the bulk

$$\frac{\epsilon_{mix}}{\epsilon_{bulk}} = \frac{1-\alpha}{1+0.5\,\alpha}, \qquad [24]$$

where ϵ_{mix} denotes the relative permittivity of the mixture, ϵ_{bulk} that of the pure bulk phase and α the overall volume fraction. The spheres are assumed to be non-interacting and hence [24] is valid only for low void fractions ($\alpha < 0.1$). From [22], with $\epsilon_1 = \epsilon_2 = \epsilon_{mix}$, the relative capacitance difference is calculated. The theoretical calibration curves for air–water dispersed flow are given in figure 10. The thickness of the wall of the acrylate inner tube can be chosen in such a way that the calibration curves is almost linear and close to the diagonal. At low void fractions the validity of the model can be verified by simulating dispersed flow with, for example, plastic beads.

Stratified flow

For a stratified flow pattern an analytical solution of the Laplace equation is not available and only experimental calibration curves are presented. To obtain the calibration curve for the 50 mm sensor, the tube is placed horizontally and filled with distilled water in 10 equal steps.

For the 5 mm sensor this method is not very accurate because the liquid is not spread out very well in the small tube. Therefore mock-ups machined from acrylate rods are used to simulate the gas. The dimensions of the mock-up are measured very precisely and from that the volume fraction of the acrylate is calculated (error $\pm$ 0.02). To examine the influence of the use of acrylate mock-ups this method is also applied to the 50 mm sensor and compared with horizontal filling.

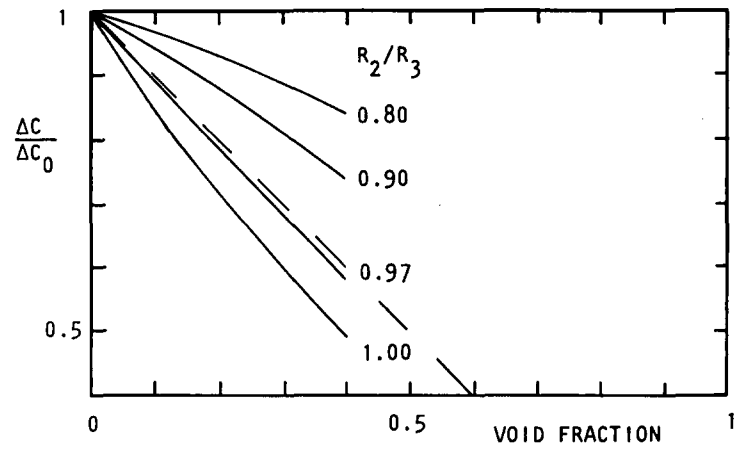

Figure 10. Calibration curves for dispersed flow.

Figures 11 and 12 show the experimental results for the 50 and 5 mm sensors. With electrodes flush with the wall the influence of the acrylate sensor tube is qualitatively the same for both sensors. The sensitivity of the device for void fractions in the range $\alpha > 0.8$ is low. By rotating the sensor or the acrylate mock-up, the RCD fluctuates by less than ± 0.01 (50 mm) and ± 0.02 (5 mm). This emphasizes the cylindrical symmetry of the sensors.

If the conductivity of the water is raised from 2.5×10^{-4} to 50×10^{-4} $1/\Omega$ m the capacitance increases by about 10%. This dispersion is known as the Maxwell–Wagner effect (Hasted 1973). The RCD however differs by <0.02 and without knowing the exact value of the specific conductivity, accurate void measurements are still possible. Also, a mixture of water with 38% glycerine ($\epsilon_r = 71$) does not significantly influence (<0.01) the course of the calibration curve.

As can be seen from figure 11 the RCD of the 50 mm sensor with acrylate mock-ups, on average, 0.06 above the calibration curve for horizontal air–water filling. The difference may be due to the following two effects. First the permittivity of acrylate is larger than that of air. The field lines are therefore more concentrated in a certain region using acrylate instead of air. Hence, with acrylate mock-ups crossing of the field lines from electrode 1 to electrode 2 is facilitated and consequently the value of the RCD is higher. The second influence is the presence of a small layer of water

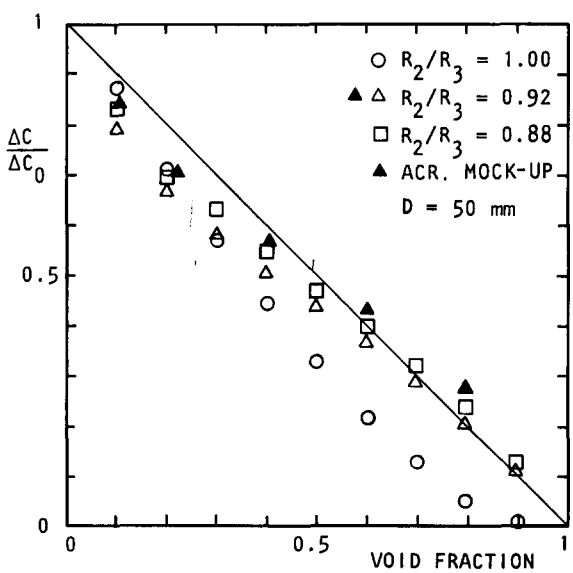

Figure 11. Calibration curves for stratified flow, 50 mm sensor.

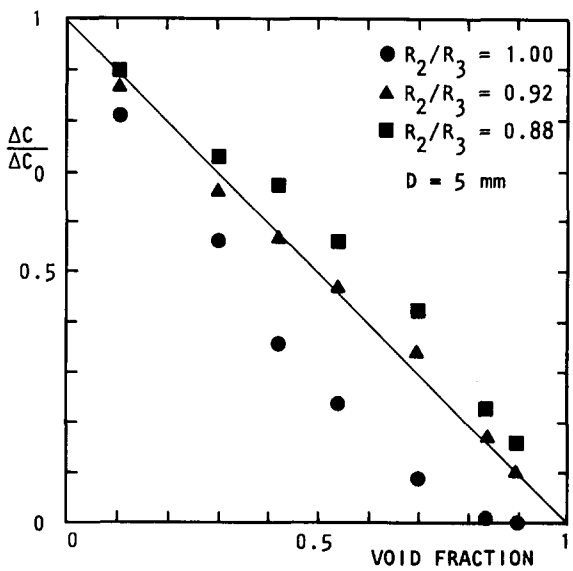

Figure 12. Calibration curves for stratified flow, 5 mm sensor.

between the mock-up and the sensor tube. The calibration curves for annular flow show that (for $R_2/R_3 = 0.88$ or 0.92) a certain volume of liquid at the wall of the tube gives a higher contribution to the RCD than the same volume in the centre of the tube. Also, from experiments it is found that the RCD for an acrylate rod placed at the centre is about 0.05 higher than at the wall. This indicates the non-linearity of the sensor and shows that, in principle, different calibration curves have to be used for the various flow regions.

Measurement strategy for intermittent flow

On behalf of the scaling tests, in addition to stratified and annular flow, 28 intermittent flows in the 5 and 50 mm tubes are compared. From the time-varying void signals it was found that in 23 of the 28 adjusted intermittent flows, the sensor is occasionally (plug/slug flow pattern) or always (plug flow pattern) completely filled with liquid during the passage of the "Plug body". Consequently, the amount of entrained gas in the slug body is very small for these flow patterns. Notice that the definition of the plug/slug flow pattern (see the next section) is different from the usual one. In the literature plug flow is often regarded as the limiting case of slug flow, where the liquid slug is almost free of entrained gas. Also, from visual observations of the 50 mm flow the number of bubbles in the flow appeared to be small in many cases, and regarding the intermittent flow as being locally stratified is therefore a reasonable assumption in the region concerned. If two flows have to be compared only, then it is sufficient that the calibration curves are identical.

The curves for annular, stratified and dispersed flows of the sensors used for the scaling tests are given in figures 13 and 14. The stratified flow curve of the 5 mm sensor (figure 14) is corrected for the use of acrylate mock-ups with calibration: the values are 0.06 lower than those (▲) of figure 12, except for $\alpha = 0$ and $\alpha = 1$. To obtain the mean void fraction the measured capacitance is averaged by integration. Because an intermittent flow contains different stratified regions and the stratified calibration curve is not linear, α is calculated from a more or less intuitively determined averaged curve. The stratified curve and partially the annular and dispersed curves determine the location of the averaged curve. For the 50 mm sensor α is calculated from

$$\alpha_{50} = 1 - \mathrm{RCD} = \frac{C_m - C_L}{C_G - C_L}, \qquad [25]$$

where the subscripts m, L and G represent mixture, liquid and gas, respectively. Equation [25] represents the diagonal in figure 13. For the 5 mm sensor a line beneath the diagonal is chosen, because the calibration curve for stratified flow is below the diagonal over the whole void range:

$$\alpha_5 = 0.96 - \mathrm{RCD} = \frac{C_m - C_L}{C_G - C_L} - 0.04. \qquad [26]$$

The largest deviation of the calibration curve for stratified flow from the dashed line in figures 13 or 14 is 0.07. The adjusted intermittent flows, however, contain stratified regions with $\alpha > 0.5$ as well as stratified regions with $\alpha < 0.5$ and errors due to the non-linear calibration curve then cancel out partially. With the help of the measured time-varying void signals (see, for example, figure 15) the likely accuracy of the mean void fraction for intermittent flows, calculated from [25] or [26], is estimated. For example, from the plug flow situation of figure 16 it can be seen that the 50 mm sensor is completely filled with liquid ($\alpha = 0$ and the deviation from the averaged curve is 0) for 10% of the time and only partially filled ($0.5 < \alpha < 0.7$ and the deviation from the averaged curve is small: < 0.02) for 80% of the time. The resulting error is estimated on 0.02. Also, for the slug flow in figure 16 the error is small: approx. 0.02. From 28 adjusted intermittent flows the absolute error appeared to be always < 0.03. If a few bubbles are present in a particular part of the flow, for instance behind a liquid slug, the capacitance of that part decreases in accordance with the curve for dispersed flow. If the pipe wall is wetted after the passage of a liquid slug, the liquid on the wall causes the capacitance to change in accordance with the annular flow curve. However, the contribution of these regions to the total capacitance is small for the experimental region concerned.

In general, if the intermittent flow is very frothy, the described method is less accurate (the values are too low). A sensor with a much smaller axial width has to be used. In the film region a stratified flow curve can be used, whereas in the slug body a dispersed curve is more appropriate.

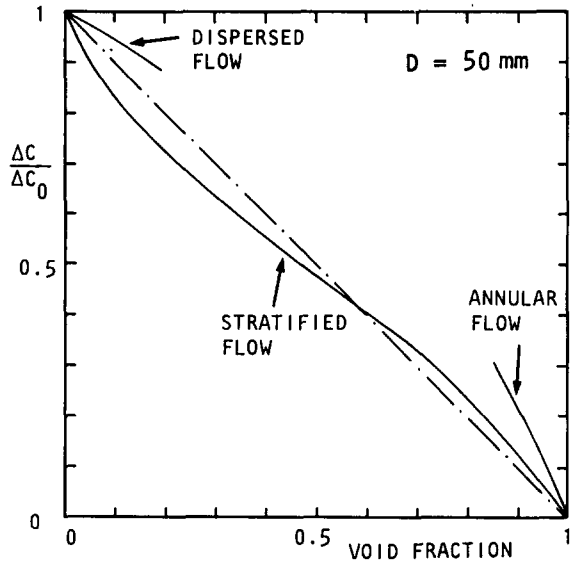

Figure 13. Calibration curves for the 50 mm sensor; for stratified and annular flow $R_2/R_3 = 0.88$, for dispersed flow $R_2/R_3 = 0.90$.

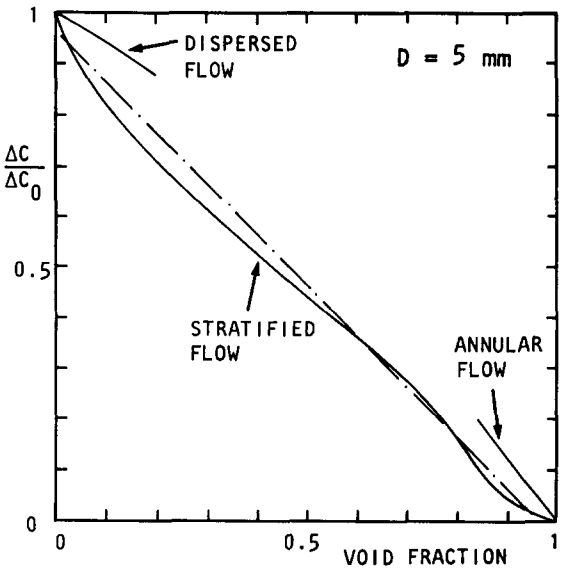

Figure 14. Calibration curves for the 5 mm sensor; for stratified and annular flow $R_2/R_3 = 0.92$, for dispersed flow $R_2/R_3 = 0.90$.

FLOW PATTERN IDENTIFICATION FROM VOID FRACTION FLUCTUATIONS

The sensors described here are also used for comparing the flow patterns. The instantaneous output signal of the capacitance meter is a measure for the void fraction in the sensor volume. The output signal of the capacitance meter is recorded with a digital oscilloscope (Nicolet 3091, sample frequency = 0.2 kHz). Figure 16 shows some recorded signals of the 50 mm flow and the 5 mm centrifugal scaled flow.

For the 50 mm section the liquid velocity is 0.4m/s and the gas velocity increases from 0.3 to 10.5 m/s; for the 5 mm section the liquid velocity is 1.3 m/s and the gas velocity increases from 1 to 35 m/s. The void signals of the 5 mm flow are flattened due to the limited response time (2 ms) of the capacitance meter.

For stratified flow the distribution of the phases in a cross-sectional plane does not change with time and hence the void fraction is constant. For ease of comparison the flow is called plug if the sensor (active length = 6 dia) is completely filled during the passage of a "liquid wave". In this case the recorded void fluctuations look like a block signal. If the sensor is called slug and the output signals resemble a sawtooth. Possibly the sawtooth signal can also be produced by roll waves. To be able to distinguish between slug flow and roll waves, a detailed comparison (with the help of visual observations) of the slug flow signal and roll wave signal is necessary. If the translation velocity is known (for example from a second sensor, placed downstream of the first sensor) then the shape and liquid content of the slug body or roll wave can be determined.

The semi-annular flow pattern is characterized by a thick liquid layer on the bottom and a thin film at the top. From visual observations in the 50 mm section it was found that the fluctuations in the void signal are caused by waves on the liquid surface and the passage of small frothy slugs. It is not slug flow, which requires a competent bridge of liquid, nor it is fully developed annular flow, which requires a stable film over the entire perimeter.

Figure 15. Idealized intermittent flow pattern.

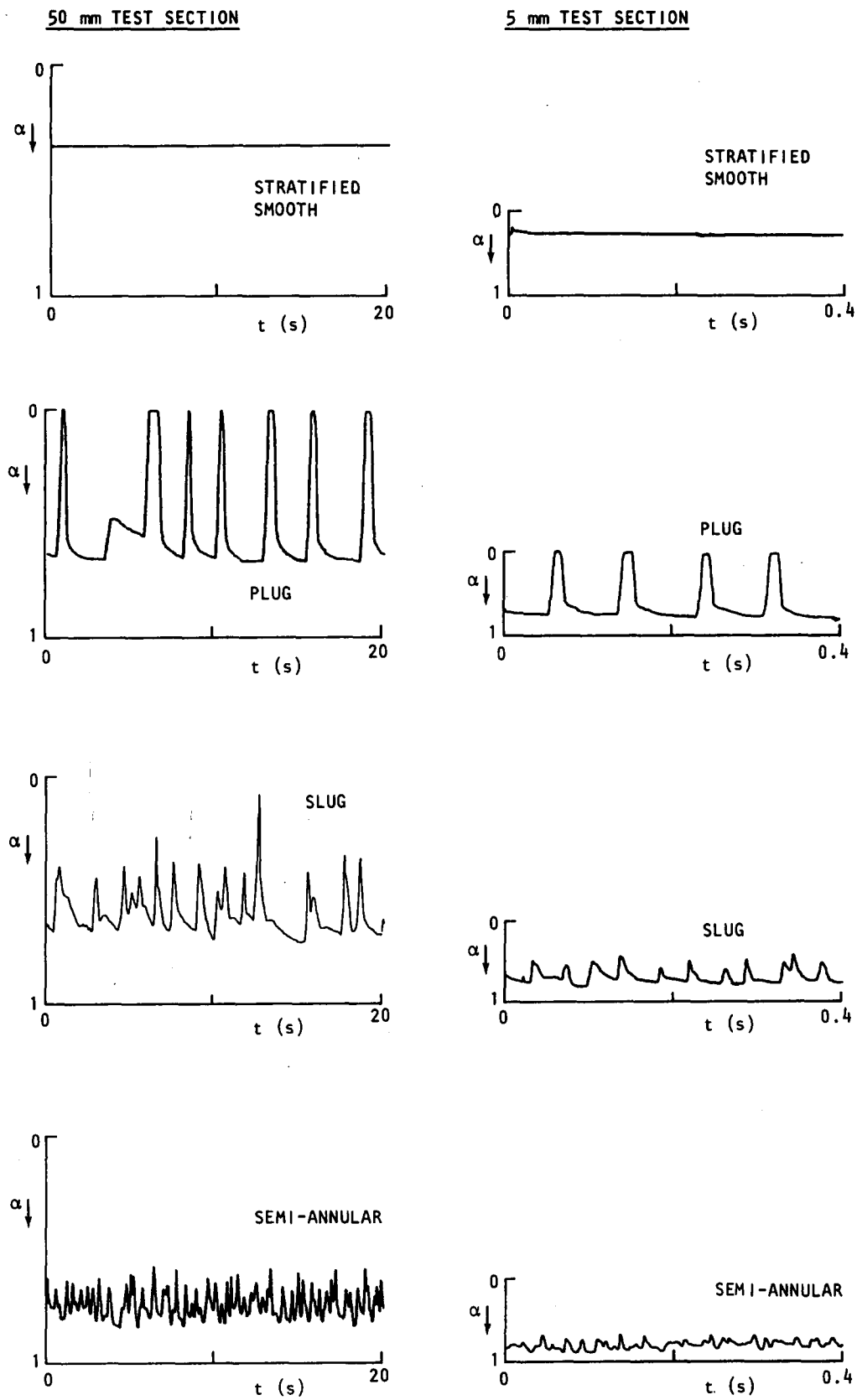

Figure 16. Void signals of the 50 and 5 mm centrifugal scaled flow. The scale of the vertical axis is not linear.

The slug and plug frequencies can be determined simply by counting the peaks in the void signal. Two slugs are detected apart if the distance between them is larger than the axial extension of the sensor: $U_s/f > 6D$, where U_s is the translation speed of the slug, f is the slug or plug frequency and $6D$ is the axial extension of the sensor (D is the inner diameter). The translation speed of a slug is about 1.3 times the sum of the superficial gas and liquid velocities (Gregory & Scott 1969; Kvernvold *et al.* 1984). Hence, the maximum frequency that can be measured is given by

$$f_{max} = 1.3 \frac{(U_L + U_G)}{6D}.$$

CONCLUSIONS

Mean phase content can be determined without disturbing the hydrodynamics of the two-phase flow. Because of the helical electrode configuration spatial averaging is automatically realized and only a standard capacitance meter is needed. Guard electrodes render edge effects negligible. The sensor is easy to machine especially for tube dia >15 mm.

For two-phase annular and dispersed flows a theoretical method is put forward for determining calibration curves for a wide range of permittivities. Only for the sensors with the electrodes flush on the wall is the quantitative agreement satisfactory. The thickness and permittivity of the dielectric sensor tube determines the course of the calibration curves to a large extent. This is confirmed by the experimental calibration curves. As long as the slug body is free or almost free of entrained gas the calibration curve for stratified flow can also be used for intermittent flow. From the time-averaged capacitance the void fraction can be determined with an accuracy of ± 0.03, provided the flow pattern is known or can be guessed. The time-varying void signal is useful for identification of the flow pattern.

Capacitance sensors with electrodes flush on the wall are less suitable for void fraction measurements because the calibration curves are not, in general, linear and for annular flow, for example, the capacitance is almost independent of the void fraction in the relevant void range ($\alpha > 0.8$). By using a dielectric inner tube with a low relative permittivity, the electric field lines are forced to cross the tube to the counter electrode. Provided the relative permittivities of the two substances involved are known, then for a particular flow pattern a linear relation between the void fraction and the relative capacitance difference can be arranged by optimizing the thickness and relative permittivity of the dielectric inner tube. If the permittivity of the two phases does not differ very much, e.g. oil and air, the sensitivity of the calibration curves to the thickness and permittivity of the sensor tube is much less than with air–water flows.

Acknowledgements—The authors acknowledge Dr W. C. Heerens of the Delft University of Technology for advice about the electrode configuration. They are greatly indebted to the technical staff of the Delft University of Technology for making the sensors.

REFERENCES

ABOUELWAFA, M. S. A. & KENDALL, E. J. M. 1979 Determination of the theoretical capacitance of a concave sensor. *Rev. Sci. Instrum.* **50,** 1158–1159.

ABOUELWAFA, M. S. A. & KENDALL, E. J. M. 1980 The use of capacitance sensors for phase percentage determination in multiphase pipelines. *IEEE Trans. Instrum. Measur.* **29,** 24–27.

BORST, J. C. 1983 Een capacitieve sensor voor gas-volumefractie metingen. Research Report, Dept of Mechanical Engineering, Delft Univ. of Technology. In Dutch.

BORST, J. C. 1985 Een capacitieve sensor voor het bepalen van gas-volumefracties in twee-fasen mengsels. M.Sc. Thesis, MEAH-Report 51, Delft Univ. of Technology. In Dutch.

CHESTERS, A. K. 1977 A note on the centrifugal scaling of horizontal isothermal, liquid–gas flows without mass transfer. *Int. J. Multiphase Flow* **3,** 235–241.

GERAETS, J. J. M. 1986 Centrifugal scaling of isothermal gas–liquid flow in horizontal tubes. Ph.D. Thesis, Delft Univ. of Technology.

GERAETS, J. J. M. 1988 Centrifugal scaling of isothermal gas–liquid flow in horizontal tubes. *Int. J. Multiphase Flow* **14,** 287–303.

GREGORY, G. A. & MATTAR, L. 1973 An *in-situ* volume fraction sensor for two-phase flow of non-electrolytes. *J. Can. Pet. Technol.* **12,** 48–52.

GREGORY, G. A. & SCOTT, D. S. 1969 Correlation of liquid slug velocity and frequency in horizontal co-current gas–liquid slug flow. *AIChE Jl* **5,** 933–935.

HASTED, J. B. 1973 *Aqueous Dielectrics*, pp. 126–131. Chapman & Hall, London.

HEERENS, W. C. & VERMEULEN, F. C. 1975 Capacitance of Kelvin guard-ring capacitors with modified edge geometry. *J. appl. Phys.* **46,** 2486–2488.

HEWITT, G. F. 1978 *Measurements of Two-phase Flow Parameters*. Academic Press, New York.

KVERNVOLD, O., VINDOY, V., SONDTVEDT, T., SAASEN, A. & SELMER-OLSEN, S. 1984 Velocity distribution in horizontal slug flow. *Int. J. Multiphase Flow* **10,** 441–457.

MAXWELL, J. C. 1881 *A Treatise on Electricity and Magnetism*, Vol. 1, 3rd edn. Clarendon Press, Oxford.

REHMAN, M., MUKERJI, S. K. & MURTI, V. G. K. 1982 Effect of a symmetrically placed dielectric tube on the capacitance of a cylindrical cross-capacitor. *Proc. IEE* **129,** 332–336.